

## Charge disproportionate antiferromagnetism at the verge of the insulator-metal transition in doped $\text{LaFeO}_3$

S. Jana,<sup>1,2,\*</sup> S. K. Panda,<sup>3,4</sup> D. Phuyal,<sup>1</sup> B. Pal,<sup>2</sup> S. Mukherjee,<sup>2,†</sup> A. Dutta,<sup>2</sup> P. Anil Kumar,<sup>5,‡</sup> D. Hedlund,<sup>5</sup> J. Schött,<sup>1</sup> P. Thunström,<sup>1</sup> Y. Kvashnin,<sup>1</sup> H. Rensmo,<sup>1</sup> M. Venkata Kamalakar,<sup>1</sup> Carlo U. Segre,<sup>6</sup> P. Svedlindh,<sup>5</sup> K. Gunnarsson,<sup>5</sup> S. Biermann,<sup>3,7</sup> O. Eriksson,<sup>1,8</sup> O. Karis,<sup>1</sup> and D. D. Sarma<sup>2,§</sup>

<sup>1</sup>*Department of Physics and Astronomy, Uppsala University, 752 36 Uppsala, Sweden*

<sup>2</sup>*Solid State and Structural Chemistry Unit, Indian Institute of Science, Bengaluru 560012, India*

<sup>3</sup>*Centre de Physique Théorique, Ecole Polytechnique, CNRS UMR 7644, Université Paris-Saclay, 91128 Palaiseau, France*

<sup>4</sup>*Department of Physics, Bennett University, Greater Noida 201310, Uttar Pradesh, India.*

<sup>5</sup>*Department of Engineering Sciences, Uppsala University, 751 21 Uppsala, Sweden*

<sup>6</sup>*CSRRI & Department of Physics, Illinois Institute of Technology, Chicago, Illinois 60616, USA*

<sup>7</sup>*Collège de France, 11 place Marcelin Berthelot, 75005 Paris, France*

<sup>8</sup>*School of Science and Technology, Örebro University, SE-70182 Örebro, Sweden*



(Received 14 March 2018; revised manuscript received 14 June 2018; published 5 February 2019)

We explore the effects of electron doping in lanthanum ferrite,  $\text{LaFeO}_3$  by doping Mo at the Fe sites. Based on magnetic, transport, scanning tunneling spectroscopy, and x-ray photoelectron spectroscopy measurements, we find that the large gap, charge-transfer, antiferromagnetic (AFM) insulator  $\text{LaFeO}_3$  becomes a small gap AFM band insulator at low Mo doping. With increasing doping concentration, Mo states, which appear around the Fermi level, is broadened and become gapless at a critical doping of 20%. Using a combination of calculations based on density functional theory plus Hubbard  $U$  (DFT+ $U$ ) and x-ray absorption spectroscopy measurements, we find that the system shows charge disproportionation (CD) in Fe ions at 25% Mo doping, where two distinct Fe sites, having  $\text{Fe}^{2+}$  and  $\text{Fe}^{3+}$  nominal charge states appear. A local breathing-type lattice distortion induces the charge disproportionation at the Fe site without destroying the antiferromagnetic order. Our combined experimental and theoretical investigations establish that the Fe states form a CD antiferromagnet at 25% Mo doping, which remains insulating, while the appearance of Mo states around the Fermi level is showing an indication towards the insulator-metal transition.

DOI: [10.1103/PhysRevB.99.075106](https://doi.org/10.1103/PhysRevB.99.075106)

Doping perovskite transition-metal oxides  $\text{ABO}_3$ , has resulted in exotic physics, such as insulator-metal transition (IMT), colossal magnetoresistance (CMR), orbital and charge ordered (CO) states. The  $A$ -site ions, usually a rare-earth or alkali-metal, provide the structural skeleton after donating electrons to the valence band, while  $B$ -site ions, usually a transition-metal and the oxygen ions are predominantly responsible for the low-energy electronic states. Often the  $A$  site is doped to either dope holes/electrons or to introduce structural changes for manipulating material properties. In particular in manganites, a large number of materials with chemical formula  $R_{1-x}A_x\text{MnO}_3$  ( $R = \text{La, Pr, or Nd}$  and  $A = \text{Ca, Br, Sr, Pb}$ ) [1,2] have been realized, where most of them exhibit CMR for  $x \sim 0.3$  [3], around the IMT where doping transforms an antiferromagnetic (AFM) charge transfer insulator to a ferromagnetic (FM) mixed-valence metallic com-

pound [4]. The physics of this transition has been attributed to the double-exchange mechanism [5–7], which promotes a FM ordering by allowing the  $e_g$  electron to hop between  $\text{Mn}^{3+}$  and  $\text{Mn}^{4+}$  ions, resulting in metallic conduction, while the insulating AFM state in the parent compound arises due to the superexchange interactions between the Mn ions. At larger values of  $x$  ( $> 0.5$ ), the metallic FM ground state transforms into a CO ground state where the  $\text{Mn}^{3+}$  and  $\text{Mn}^{4+}$  ions order spatially in the crystalline lattice [8,9], suppressing the double exchange and thus favoring AFM ordering due to superexchange interaction [10,11]. Thus the insulating state always coexists with the AFM ordering and metallic conduction appears to be a prerequisite for the ferromagnetism in these compounds.

In strong similarity with manganites, the perovskite ferrites  $\text{AFeO}_3$  ( $A = \text{Lu, Eu, Y, Pr, and La}$ ) [12–15] are typically high-spin ( $\text{Fe}^{3+}$ ,  $S = 5/2$ ), wide-gap insulators with AFM ground states [16–18]. Several attempts have been made to realize IMT and other phenomena in ferrites too, following the above-mentioned route of  $A$ -site substitution [19–21]. Among the most studied ferrites,  $\text{LaFeO}_3$  has been hole doped, but unlike the corresponding manganite,  $\text{La}_{1-x}\text{Sr}_x\text{FeO}_3$  retains an insulating AFM state even up to 40% Sr substitution, establishing the robustness of the antiferromagnetism in this compound [21]. These results emphasize that even at  $x = 0.4$ ,

\*Present Address: Helmholtz-Zentrum Berlin (FG-ISRR), Albert Einstein Straße 15, 12489 Berlin, Germany; sj.phys@gmail.com

†Present Address: Department of Physics and Astronomy, Uppsala University, 752 36 Uppsala, Sweden.

‡Present Address: Seagate Technology, 1 Disc Drive, Springtown, Northern Ireland BT48 0BF, United Kingdom.

§sarma@iisc.ac.in

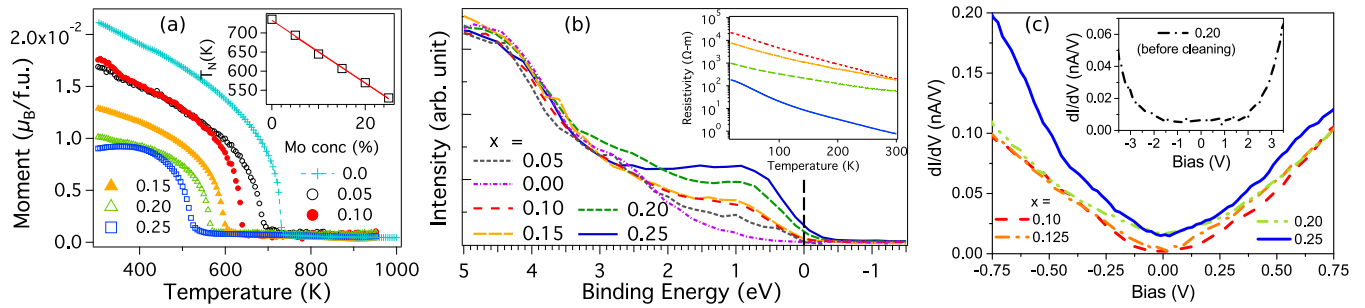


FIG. 1. (a) Temperature dependence of the magnetization for all investigated compositions. Inset: The variation of antiferromagnetic transition temperature ( $T_N$ ) as a function of doping ( $x$ ). (b) Valence band photoelectron spectra, normalized to the La  $5p_{3/2}$  peak ( $\sim 17.7$  eV) for all the compositions. Inset: The resistivity vs temperature plots for  $x = 0.10, 0.15, 0.20, 0.25$ . (c) Scanning tunneling spectroscopic (STS) data collected at room temperature in an UHV system using a variable temperature STM system. Standard ac modulation technique was used for STS measurements with an ac modulation amplitude of 10 mV and frequency 2731 Hz. The  $dI/dV$  spectra for  $x = 0.10, 0.125, 0.20, 0.25$  compositions are plotted. Inset shows the same for uncleaned  $x = 0.20$  sample. Tunnel spectra were taken at different locations over  $2 \times 2$  mm<sup>2</sup> area on each composition and the plotted spectra is the spatial average of all of them.

the doped hole states do not achieve enough bandwidth to overlap with the top of the valence band. At higher doping around  $x = 0.7$ , CD occurs on the Fe sites ( $\text{Fe}^{3+}$  and  $\text{Fe}^{5+}$ ) at low temperature, resulting in an insulating AFM ground state [22,23]. *B*-site doping has also been explored [24–28]. Idrees *et al.* [26] report that even 50% Ni doping in  $\text{LaFeO}_3$  ( $\text{LaFe}_{1-x}\text{Ni}_x\text{O}_3$ ) could not destabilize the insulating AFM state.

The coexistence of AFM order and metallicity is extremely rare in perovskite oxides. However, the search for such an exotic state has continued to draw significant attention since the discovery of high- $T_c$  superconductivity in copper oxides. Since a few studies indicate the robustness of antiferromagnetism in  $\text{LaFeO}_3$  [21,26], the possibility of a novel metallic AFM state could be explored through appropriate *B*-site substitution. Since *4d* elements such as Mo have much broader *d* bands, this comes as a natural choice.

To obtain an IMT, without an associated magnetic transition in a wide-gap perovskite oxide, this work focuses on electron doping in bulk  $\text{LaFe}_{1-x}\text{Mo}_x\text{O}_3$  (LFMO- $x$ ). Based on magnetic, transport, x-ray spectroscopy measurements and DFT+U calculations, we investigate the variation of electronic and magnetic properties as a function of  $x$  and establish that the system starts showing spectral weight at the Fermi level for  $x \geq 0.20$ . The theoretical analysis of 25% Mo-doped system proposes CD in the Fe sites, where two different types of Fe ions, assuming 2+ and 3+ valence states, form the insulating network, while the Mo states appear at and around the Fermi level. The proposed CD state has been verified from x-ray absorption spectroscopy (XAS) and extended x-ray absorption fine structure analysis, providing conclusive evidence of CD, AFM ground state on the verge of insulator-metal transition.

Six samples of LFMO- $x$  ( $x = 0.00, 0.05, 0.10, 0.15, 0.20, 0.25$ ) are studied. We could not make samples beyond  $x = 0.25$  in pure form within the thermodynamically equilibrium synthesis conditions. Phase purity and the highly crystalline nature of the samples were confirmed by x-ray diffraction (see Supplemental Material (SM) [29]). Figure 1(a) shows the magnetization ( $M$ ) as a function of temperature for all compositions. The data is measured while cooling in an

applied field of 1000 Oe. The AFM transition temperature ( $T_N$ ) of  $\text{LaFeO}_3$  agrees well with the previously reported value [47]. The  $T_N$  is observed to decrease linearly with increasing Mo doping [see inset of Fig. 1(a)], while the ferromagnetic (FM)-like saturation of the moment below  $T_N$  is typically observed due to the small canting of the moments at relatively high applied field [47]. These results indicate that even at the highest doping, the system remains antiferromagnetic.

Next, the spectral function at  $E_F$  is examined by means of valence-band photoelectron spectroscopy (PES) conducted at room temperature (RT) as displayed in Fig. 1(b). All spectra are energy calibrated relative to a Au reference measured under identical conditions and intensities are normalized relative to the La  $5p_{3/2}$  peak (17.7 eV). For the undoped sample, a large gap between  $E_F$  and the top of the valence band is present, while with the Mo doping, electronic states start to appear in the gap. For  $x = 0.05, 0.10$ , and  $0.15$  samples, the tail of the valence band is ending below  $E_F$ , i.e., no DOS at  $E_F$ . However, for  $x = 0.20$  and  $0.25$  samples, clearly, a sizable number of states appear at  $E_F$ .

The resistivity ( $\rho$ ) data is displayed in the inset of Fig. 1(b). We note that resistivity of the pure  $\text{LaFeO}_3$  is as high that we could not measure it due to the limitation in our setup. Although the resistivity data reveals a two order of magnitude reduction in the magnitude for LFMO-0.25 compared to the LFMO-0.10 composition,  $\partial\rho/\partial T$  is still negative. However, the  $\rho(T)$  of LFMO-0.25 does not diverge at low temperature like the typical insulating samples. The negative  $\partial\rho/\partial T$  has been reported in other metallic systems such as ferromagnetic  $\text{CrO}_2$  [48] and antiferromagnetic  $\text{CaCrO}_3$  [49,50], which is considered to be in the crossover regime between localized and itinerant electrons [51] as in our system. The reason has been attributed to the domination of the insulating grain boundaries in the polycrystalline sample [48,49]. We will illustrate below that this is likely to be the case for our system.

To further investigate the states at and around the Fermi level, the scanning tunneling spectroscopy (STS) measurements are carried out as displayed in Fig. 1(c). Our results show a finite  $dI/dV$  at zero bias ( $V = 0$ ) for both 20% and 25% Mo doping, indicating finite DOS at the Fermi level ( $E_F$ ) for both samples, while negligible  $dI/dV$  at  $V = 0$  for

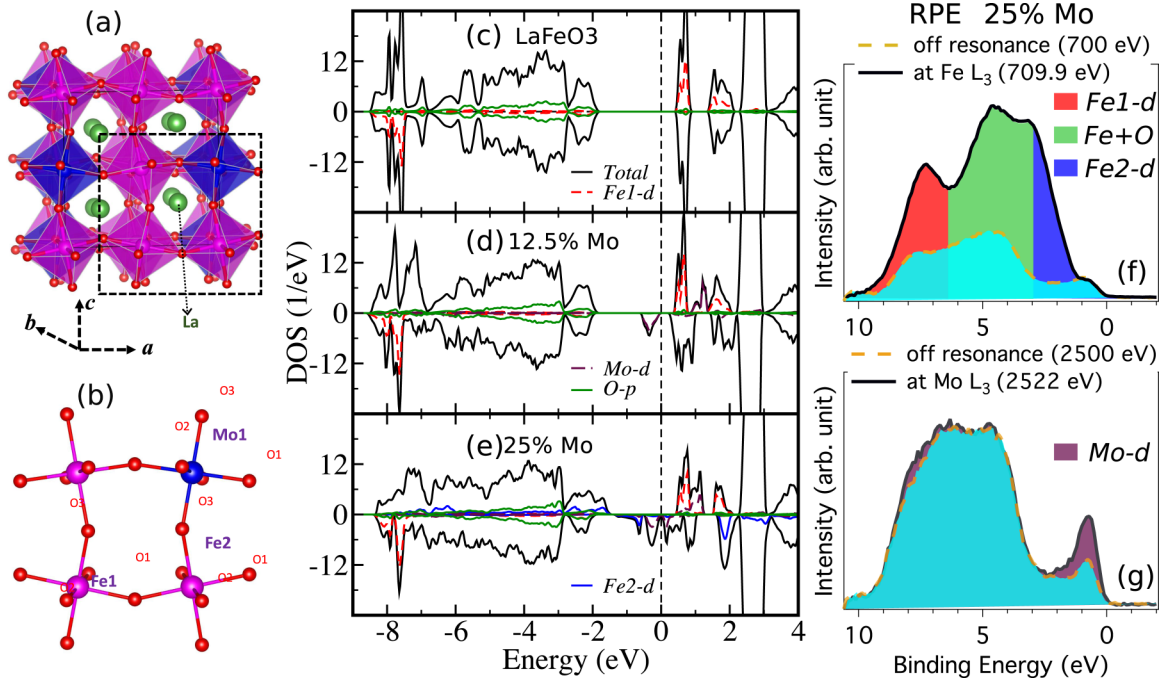


FIG. 2. (a) The schematic of the  $\sqrt{2} \times \sqrt{2}$  supercell, considered for theoretical simulations of  $x = 0.25$  sample, consisting of six Fe and two Mo ions. The Mo ions are substitutes at the Fe sites and this particular arrangement of Mo ions is energetically favorable (see SM [29]). (b) The dotted part of the structure in (a) is highlighted for a better visualization of the two kinds of Fe ions (Fe1, and Fe2), present in the relaxed structure of 25% doped sample. Our optimized structure within DFT+U approach find that all the six bonds in Fe1-O<sub>6</sub> octahedra are almost equal to their corresponding values in pure LaFeO<sub>3</sub> (2.02 Å), while four Fe-O bonds are larger (2.07 Å) in Fe2O<sub>6</sub> octahedra, indicating a breathing-type lattice distortion. DFT+U total (black solid line), partial density of states of the Fe1-*d* (red solid line), Mo-*d* (maroon dotted line), O-*p* (blue solid line), and Fe2-*d* (blue solid line) in the AFM ground state of LaFe<sub>1-x</sub>Mo<sub>x</sub>O<sub>3</sub> corresponding to (c)  $x = 0.0$ , (d)  $x = 0.125$ , and (e)  $x = 0.25$ . The Fermi level for LaFeO<sub>3</sub> has been assigned in such a way that Fe-*d* states appear at a binding energy consistent with our experimental resonance photoemission spectra (RPES). The RPES spectra obtained at (f) Fe-L<sub>3</sub> and (g) Mo-L<sub>3</sub> edge for  $x = 0.25$  composition. The off and on resonance spectra for Fe (Mo) were collected when the excitation energy was set at 700 eV (2500 eV) and 709.9 eV (2522 eV), respectively. The important spectral features of the electronic states of (e) are identified from RPES data.

10% and 12.5% Mo doping, supporting our observation from the PES measurements. The inset of Fig. 1(c), showing the  $dI/dV$ - $V$  curve measured on the uncleaned 20% Mo-doped sample, demonstrates the insulating nature of the grain boundary, as  $dI/dV$  remains negligibly small for large range of  $V$ . Therefore, the insulating nature of the grain boundary could be the reason of negative  $\partial\rho/dT$ . We note here that resistivity measurement on a single crystal could provide more insight into it, which is beyond the scope of this paper.

To understand the mechanism of the evolution of the electronic and magnetic states as a function of doping, we calculate the electronic structure of  $x = 0.00$ , 0.125, and 0.25 samples by means of DFT+U (density functional theory + Hubbard  $U$ ) approach as implemented in the WIEN2K code [52,53]. The constrained random phase approximation (cRPA) method has been employed to estimate the effective Coulomb interaction parameters (Hubbard  $U$  and Hund's  $J$ ) for the Fe-3*d* states in order to make our approach truly *ab initio*. The estimated  $U$  and  $J$  for Fe-*d* states are, respectively, 4.4 eV and 0.7 eV. The technical details of all these calculations are provided in the SM [29]. Experimentally, LaFeO<sub>3</sub> ( $x = 0.00$ ) forms in the orthorhombic crystal structure with space group  $Pnma$  [54]. We consider a  $\sqrt{2} \times 1 \times \sqrt{2}$  cell to simulate two different doping concentrations. The cell for  $x = 0.25$  (six Fe and two Mo) is displayed in Fig. 2(a). This specific

arrangement of the Mo ions are found to be lowest in energy (see SM [29]), while Mo replaces Fe completely disorderly as probed by XRD and EXAFS (see SM [29]). The optimized structure reveals that Mo doping produces two types of Fe atoms [Fe1 and Fe2 in Fig. 2(b)]. The Fe1 is surrounded by only Fe ions as in pure LaFeO<sub>3</sub> and thus all the six Fe1-O bond distances remain almost equal to their corresponding values in pure compound (2.02 Å), while in the Fe2O<sub>6</sub> octahedra, the presence of nearest Mo ions makes Fe2-O2 and Fe2-O3 (total four bonds) distances equal to 2.07 Å. Such breathing-type lattice distortion has been attributed as the cause of CD state in many rare-earth nickelate perovskites [55,56] and also in CaFeO<sub>3</sub> [14]. Since a very similar Fe-O bond disproportionation or breathing distortion is observed in the present system, it strongly indicates the possibility of such novel state.

We analyze the total and projected DOS of the AFM ground state for both the pure and two doped systems. We note that the AFM-I state is found to be the lowest-energy state as described in the SM [29]. The total DOS of pure LaFeO<sub>3</sub>, displayed in Fig. 2(c), reveals that the magnetic ground state is a wide gap insulator. The calculated band gap is 2.25 eV, which is in good agreement with the experimental value of 2.0–2.2 eV [21,57]. This justifies the numerical accuracy of our estimated  $U$  and  $J$  since the calculated band gap depends on the choice of  $U$  [58,59]. A large exchange

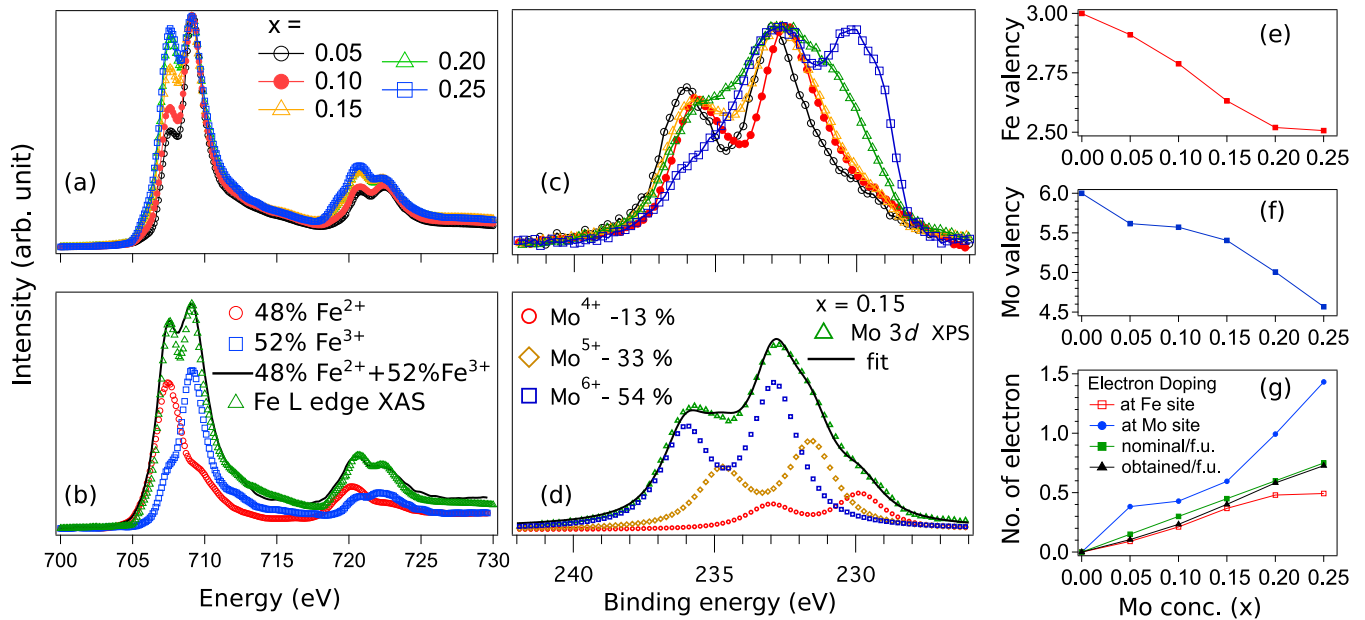


FIG. 3. (a) Fe  $L$  edge XAS spectra for all the compositions. (b) Fitted data for  $x = 0.20$  sample by the weighted average of the reference spectra of  $\text{Fe}^{2+}$  and  $\text{Fe}^{3+}$ . (c) Mo  $3d$  core level XPS spectra. (d) Experimental (open triangle), and fitted (solid line) spectra for  $x = 0.15$  and the contributions from  $\text{Mo}^{6+}$ ,  $\text{Mo}^{5+}$ , and  $\text{Mo}^{4+}$ . (e) Valency of Fe. (f) Valency of Mo. (g) Different contributions of doped electrons obtained at Fe band, Mo band, the total/f.u. and nominal/f.u. are shown.

splitting between the two spin channels of Fe- $3d$  is evident from the partial DOS (PDOS) in Fig. 2(d). One of the spin channels of Fe- $3d$  is found to be completely occupied, while the other channel is completely empty, opening up a charge transfer gap between the O- $2p$  and Fe- $3d$  states.

A major modification of the electronic structure is observed upon Mo doping as displayed in Figs. 2(d) and 2(e), for 12.5% and 25% dopant concentrations, respectively. The total DOS corresponding to the 12.5% Mo doping shows a strong reduction of the band gap to 0.23 eV. The occupied part of the Mo- $d$  states appears just below the Fermi level, which is exactly what we observe in experiment with 10% and 15% Mo-doped samples [see Fig. 1(b)], resulting in a small  $d$ - $d$  gap insulating ground state. Upon increasing the Mo concentration to 25%, the gap disappears, which lends strong support to our experimental finding. The Mo- $d$  states get broadened and eventually merge with the conduction states, while the occupied Fe- $3d$  states remain localized, located at several eV below the Fermi level.

Further the PDOSs of two types of Fe show two different charge states as expected from the analysis of the crystal geometry. We find that the  $3d$  states of the Fe1 are very similar to that of the pure  $\text{LaFeO}_3$ , implying a 3+ charge state for Fe1, while Fe2 exhibits distinctly different electronic structure. The majority  $3d$  states of Fe2 are completely occupied, while the minority states are partially filled. This is in contrast to the Fe1 where the minority channel is completely empty, giving rise to a  $2+$  ( $3d^6$ )  $S = 2$  high-spin state for Fe2. Thus the electronic structure confirms the CD state of Fe ions in 25% Mo-doped  $\text{LaFeO}_3$ , as was indicated from the observed breathing distortion.

The theoretical finding is complemented by probing the orbital characters of various VB features using resonant PES (RPES) at the Fe  $L_3$  and Mo  $L_3$  absorption edges for the

$x = 0.25$  sample, which are shown in Figs. 2(f), and 2(g), respectively. The off and on resonance VB spectra are collected at 700 eV (2500 eV) and 709.9 eV (2522 eV) for Fe  $L_3$  (Mo  $L_3$ ) edges, respectively. No noticeable resonance effects are observed at  $E_F$  for Fe, while a large enhancement of the spectral weight at  $E_F$  in the spectra recorded at the Mo  $L_3$  resonance photon energy is evident. This indicates that the Mo  $d$  states are located around  $E_F$ , which is consistent with the calculated spectra of Fig. 2(e). Comparing the PDOS with the RPES, we could also identify different Fe features as follows: dominant Fe  $2e_g$  states are between 1–3 eV; hybridized Fe and O states are between 3–6.5 eV and Fe1+Fe2  $t_{2g}$  states are between 6.5–9 eV binding energy [compare Fig. 2(e) with Figs. 2(f) and 2(g)].

To verify the theoretically proposed CD ground state, Fe and Mo valency have been probed. We probe the doping dependence of the valency of the Fe ions by means of Fe  $L$  edge x-ray XAS as displayed in Fig. 3(a). Both the  $L_3$  and  $L_2$  edges exhibit a particular trend in the spectral features, while being more prominent at the  $L_3$  edge. The  $L_3$  edge is composed of two peaks. As evidenced from the reference spectra in Fig. 3(b) [60], the lower-energy peak is predominantly  $\text{Fe}^{2+}$  while the peak at higher photon energy is attributed to  $\text{Fe}^{3+}$ . A weighted sum of the reference spectra of  $\text{Fe}^{2+}$  and  $\text{Fe}^{3+}$  is used to model and fit the experimental data to extract the average valency of Fe for each composition. The model spectrum for the 20% Mo-doped sample [Fig. 3(b)] exhibits excellent agreement with all the experimental features although it is slightly broadened due to poorer spectral resolution of the reference spectra. We note here that our calculated XAS (see SM [29]) by means of a combination of density functional theory and multiplet ligand-field theory nicely reproduces the observations shown in Figs. 3(a) and 3(b).

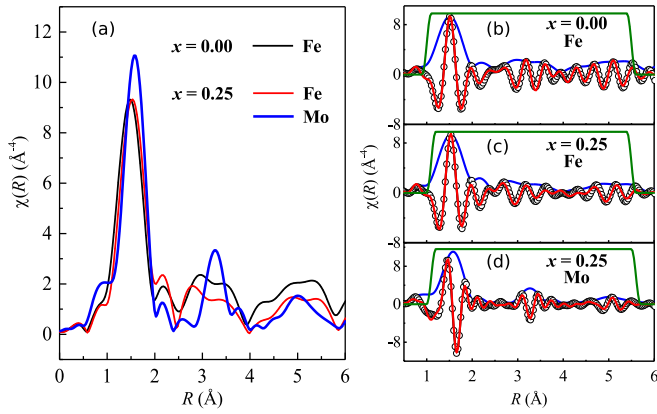


FIG. 4. (a) Magnitude of  $\chi(R)$  for Fe-K EXAFS ( $x = 0.0$ , black and  $x = 0.25$ , red) and Mo-K EXAFS ( $x = 0.25$ , blue) collected at room temperature. Fits (red curves) to the real part of  $\chi(R)$  (black open circles) for (b) Fe ( $x = 0.0$ ), (c) Fe ( $x = 0.25$ ), and (d) Mo ( $x = 0.25$ ). The corresponding magnitude of  $\chi(R)$  for each data is presented in blue. The Hanning window function (olive) has been used over the range  $1.1 \text{ \AA}$  to  $5.5 \text{ \AA}$  for the fits.

The valency of Mo is probed via  $3d$  core level PES. Figure 3(c) shows the background corrected spectra, normalized to match at maximum intensity, for all compositions. The spectra are fitted considering different valencies. A satisfactory description of the spectral features is achieved only when three Mo valencies,  $6+$ ,  $5+$ , and  $4+$ , are taken into account. Figure 3(d) shows the fitting and the corresponding contribution from different valency of Mo for the  $x = 0.15$  sample, while the same analysis for the other compositions and the details of the fittings are presented in the SM [29].

The average valency of a Fe and Mo ions derived from the fits is plotted in Figs. 3(e) and 3(f), respectively. Three electrons are donated to the system when a Fe atom ( $[Ar]3d^64s^2$ ) is replaced by Mo ( $[Kr]4d^55s^1$ ). Fe is in a  $3+$  valency ( $[Ar]3d^54s^0$ ) in the parent compound, while Mo is most stable in  $6+$  valency ( $[Kr]4d^05s^0$ ) when all the outer electrons are donated. The obtained numbers of doped electrons at the Fe and Mo sites relative to their most stable valency of  $3+$  and  $6+$ , respectively, are plotted in Fig. 3(g). The total number of doped electrons/formula unit, i.e., the sum of doped electrons at Fe and Mo sites per formula unit, match the nominal values, [see Fig. 3(g)] demonstrating the accuracy of our employed techniques. With increasing  $x$ , electrons are filled in both Fe and Mo bands [Fig. 3(g)]. However, the electron doping rate at the Fe sites reduces after  $x = 0.15$  and saturates to  $\sim 0.5/\text{f.u.}$  for  $x \geq 0.20$ . As a result, a large increase of electron doping at the Mo sites is observed for the  $x = 0.20$  sample. Further inclusion of the Mo ions, i.e., as for the case of the  $x = 0.25$  sample, pushes all additional charge to the Mo sites. This is evident from both Fe- $2p$  XAS and Mo- $3d$  PES. The Fe- $2p$  XAS remain almost identical for the  $x = 0.20$  and  $0.25$  samples [Fig. 3(a)], while the Mo- $3d$  PES show a sudden increase of the spectral weight around  $330 \text{ eV}$  corresponding to a relative increase of the  $4+$  state of Mo [Fig. 3(c)]. These observations imply that the electron doping at the Fe sites reaches the percolation threshold when the valency becomes  $2.5+$  beyond  $20\%$  Mo doping. The  $2.5+$  valency of Fe may

imply equal sharing of one electron between two Fe sites. However, as both our theoretical and experimental findings suggest, the Fe sector to be insulating, the electrons at the Fe sites are localized, which implies an equal number of  $\text{Fe}^{+3}$  and  $\text{Fe}^{+2}$  ions in the system for the  $x = 0.25$  sample.

Further, the decisive test of the two types of Fe-O bond lengths in  $25\%$  Mo-doped sample has been done by x-ray absorption fine structure (XAFS) measurements at RT (see SM for details [29]). The magnitude of Fourier transforms to the  $\chi(R)$  data for Fe-K and Mo-K EXAFS and the fits to the corresponding real part of the  $\chi(R)$  data are shown in Fig. 4. Details of the local parameters extracted from EXAFS fitting are presented in Table II in SM [29]. The two Fe-O distances, which in pure  $\text{LaFeO}_3$  differs by only  $0.024 \text{ \AA}$ , has been increased to  $0.044 \text{ \AA}$  in  $25\%$  Mo doping, which is in excellent agreement with the theoretical value of  $0.05 \text{ \AA}$ .

In summary, we have studied the evolution of the electronic and magnetic states as a function of Mo doping at the Fe site in  $\text{LaFeO}_3$  using a combination of experimental and theoretical techniques. The large gap charge transfer antiferromagnetic insulator  $\text{LaFeO}_3$  is found not to exhibit any magnetic phase transition as a function of doping, while a drastic modification of the electronic structure is observed. In particular, the ground-state electronic structure above  $20\%$  Mo doping is very unique due to its site-selective behavior: the Fe sector remains insulating having two types of Fe in the unit cell ( $\text{Fe}^{3+}$  and  $\text{Fe}^{2+}$ ), while the broad Mo  $t_{2g}$  bands started appearing at the Fermi level. Such electronic structure has been highly discussed in the literature and referred to as orbital selective Mott insulator, where nearly itinerant and localized orbitals reside on different atomic sites with  $3d$  and  $4d$  types bands, respectively. The transition to the localized state on the Fe sites is driven by the CD, while more extended and thus less correlated Mo  $4d$  band provides the states near the Fermi level. On general grounds, in such a system, exotic metallic behavior (including non-Fermi liquid properties) [61] could be expected if the pure bulk intrinsic resistivity was accessible to experimental measurements. Thus, despite observing finite spectral weight at Fermi level from valence-band PES, STS measurements and electronic structure calculations, insulator-metal transition for  $x = 0.25$  is still not fully conclusive due to the insulating behavior of the temperature dependence of the resistivity. The insulating nature of the grain boundary of our polycrystalline sample could be one of the reasons of such erroneous behavior. However, we conclude that bulk intrinsic resistivity measurement on single crystal is required to resolve this issue, which is the subject of our future study.

This work was supported by the Swedish Research Council (Grant No. 2016-4524), Knut and Alice Wallenberg Foundation (2012.0031), Swedish Energy Agency (P43294-1), and Tryggers Foundation (CTS-17:376). We thank Diamond Synchrotron and MAXII for their allocation of beamtime. We thank Department of Science and Technology, Government of India, for funding this investigation. This work was supported by a Consolidator Grant of the European Research Council (Project CorrelMat-617196), and IDRIS/GENCI Orsay (Project No. t2018091393). We thank the computer support team of CPHT for assistance. A.D. acknowledges SERB,

India, for National Post-Doctoral Fellowship. M.V.K. acknowledges the VR starting Grant No. 2016-03278 from the Swedish Research Council. O.E. acknowledges support

from the Swedish Research Council (VR), the foundation for strategic research (SSF), eSSSENCE and STandUpp. D.D.S. thanks Jamsetji Tata Trust for support.

- [1] B. Raveau, A. Maignan, C. Martin, and M. Hervieu, *Chem. Mater.* **10**, 2641 (1998).
- [2] J. M. D. Coey, M. Viret, and S. von Molnár, *Adv. Phys.* **48**, 167 (1999).
- [3] M. B. Salamon and M. Jaime, *Rev. Mod. Phys.* **73**, 583 (2001).
- [4] A. Urushibara, Y. Moritomo, T. Arima, A. Asamitsu, G. Kido, and Y. Tokura, *Phys. Rev. B* **51**, 14103 (1995).
- [5] C. Zener, *Phys. Rev.* **81**, 440 (1951).
- [6] C. Zener, *Phys. Rev.* **82**, 403 (1951).
- [7] P. W. Anderson and H. Hasegawa, *Phys. Rev.* **100**, 675 (1955).
- [8] A. P. Ramirez, P. Schiffer, S.-W. Cheong, C. H. Chen, W. Bao, T. T. M. Palstra, P. L. Gammel, D. J. Bishop, and B. Zegarski, *Phys. Rev. Lett.* **76**, 3188 (1996).
- [9] C. H. Chen and S.-W. Cheong, *Phys. Rev. Lett.* **76**, 4042 (1996).
- [10] E. O. Wollan and W. C. Koehler, *Phys. Rev.* **100**, 545 (1955).
- [11] W. Bao, J. D. Axe, C. H. Chen, and S.-W. Cheong, *Phys. Rev. Lett.* **78**, 543 (1997).
- [12] S. Ishiwata, M. Tokunaga, Y. Kaneko, D. Okuyama, Y. Tokunaga, S. Wakimoto, K. Kakurai, T. Arima, Y. Taguchi, and Y. Tokura, *Phys. Rev. B* **84**, 054427 (2011).
- [13] A. Lebon, P. Adler, C. Bernhard, A. V. Boris, A. V. Pimenov, A. Maljuk, C. T. Lin, C. Ulrich, and B. Keimer, *Phys. Rev. Lett.* **92**, 037202 (2004).
- [14] P. M. Woodward, D. E. Cox, E. Moshopoulou, A. W. Sleight, and S. Morimoto, *Phys. Rev. B* **62**, 844 (2000).
- [15] N. Hayashi, T. Yamamoto, H. Kageyama, M. Nishi, Y. Watanabe, T. Kawakami, Y. Matsushita, A. Fujimori, and M. Takano, *Angew. Chem., Int. Ed.* **50**, 12547 (2011).
- [16] R. L. White, *J. Appl. Phys.* **40**, 1061 (1969).
- [17] F. J. Kahn, P. S. Pershan, and J. P. Remeika, *Phys. Rev.* **186**, 891 (1969).
- [18] W. M. Xu, O. Naaman, G. K. Rozenberg, M. P. Pasternak, and R. D. Taylor, *Phys. Rev. B* **64**, 094411 (2001).
- [19] U. Shimony and J. M. Knudsen, *Phys. Rev.* **144**, 361 (1966).
- [20] J. Q. Li, Y. Matsui, S. K. Park, and Y. Tokura, *Phys. Rev. Lett.* **79**, 297 (1997).
- [21] A. Chainani, M. Mathew, and D. D. Sarma, *Phys. Rev. B* **48**, 14818 (1993).
- [22] M. Takano, J. Kawachi, N. Nakanishi, and Y. Takeda, *J. Solid State Chem.* **39**, 75 (1981).
- [23] R. J. McQueeney, J. Ma, S. Chang, J.-Q. Yan, M. Hehlen, and F. Trouw, *Phys. Rev. Lett.* **98**, 126402 (2007).
- [24] D. D. Sarma, A. Chainani, S. R. Krishnakumar, E. Vescovo, C. Carbone, W. Eberhardt, O. Rader, C. Jung, C. Hellwig, W. Gudat, H. Srikanth, and A. K. Raychaudhuri, *Phys. Rev. Lett.* **80**, 4004 (1998).
- [25] D. D. Sarma, O. Rader, T. Kachel, A. Chainani, M. Mathew, K. Hollmack, W. Gudat, and W. Eberhardt, *Phys. Rev. B* **49**, 14238 (1994).
- [26] M. Idrees, M. Nadeem, M. Mehmood, M. Atif, K. H. Chae, and M. M. Hassan, *J. Phys. D* **44**, 105401 (2011).
- [27] A. Chainani, D. D. Sarma, I. Das, and E. V. Sampathkumaran, *J. Phys.: Condens. Matter* **8**, L631 (1996).
- [28] M. Abbate, G. Zampieri, J. Okamoto, A. Fujimori, S. Kawasaki, and M. Takano, *Phys. Rev. B* **65**, 165120 (2002).
- [29] See Supplemental Material at <http://link.aps.org/supplemental/10.1103/PhysRevB.99.075106>, which includes Refs. [30–46], technical details of sample preparations, experimental measurements and theoretical calculations. A few supportive data from XRD, XAFS, XAS, RPES measurements, and theoretically calculated non-spin-polarized electronic structure as well as XAS are also provided in the Supplemental Material.
- [30] J. Rodríguez-Carvajal, *Physica B: Condensed Matter* **192**, 55 (1993).
- [31] B. Ravel and M. Newville, *J. Synch. Rad.* **12**, 537 (2005).
- [32] S. I. Zabinsky, J. J. Rehr, A. Ankudinov, R. C. Albers, and M. J. Eller, *Phys. Rev. B* **52**, 2995 (1995).
- [33] J. Baltrusaitis, B. Mendoza-Sanchez, V. Fernandez, R. Veenstra, N. Dukstiene, A. Roberts, and N. Fairley, *Appl. Surf. Sci.* **326**, 151 (2015).
- [34] J. P. Perdew, K. Burke, and M. Ernzerhof, *Phys. Rev. Lett.* **77**, 3865 (1996).
- [35] F. Aryasetiawan, M. Imada, A. Georges, G. Kotliar, S. Biermann, and A. I. Lichtenstein, *Phys. Rev. B* **70**, 195104 (2004).
- [36] L. Vaugier, H. Jiang, and S. Biermann, *Phys. Rev. B* **86**, 165105 (2012).
- [37] C. Martins, M. Aichhorn, L. Vaugier, and S. Biermann, *Phys. Rev. Lett.* **107**, 266404 (2011).
- [38] Y. Nomura, M. Kaltak, K. Nakamura, C. Taranto, S. Sakai, A. Toschi, R. Arita, K. Held, G. Kresse, and M. Imada, *Phys. Rev. B* **86**, 085117 (2012).
- [39] B. Amadon, T. Applencourt, and F. Bruneval, *Phys. Rev. B* **89**, 125110 (2014).
- [40] A. van Roekeghem, L. Vaugier, H. Jiang, and S. Biermann, *Phys. Rev. B* **94**, 125147 (2016).
- [41] S. K. Panda, H. Jiang, and S. Biermann, *Phys. Rev. B* **96**, 045137 (2017).
- [42] P. Seth, P. Hansmann, A. van Roekeghem, L. Vaugier, and S. Biermann, *Phys. Rev. Lett.* **119**, 056401 (2017).
- [43] G. Kresse and J. Hafner, *Phys. Rev. B* **47**, 558 (1993).
- [44] G. Kresse and J. Furthmüller, *Phys. Rev. B* **54**, 11169 (1996).
- [45] M. W. Haverkort, M. Zwierzycki, and O. K. Andersen, *Phys. Rev. B* **85**, 165113 (2012).
- [46] J. Lüder, J. Schött, B. Brena, M. W. Haverkort, P. Thunström, O. Eriksson, B. Sanyal, I. Di Marco, and Y. O. Kvashnin, *Phys. Rev. B* **96**, 245131 (2017).
- [47] S. Ivanov, R. Tellgren, F. Porcher, T. Ericsson, A. Mosunov, P. Beran, S. Korchagina, P. A. Kumar, R. Mathieu, and P. Nordblad, *Mater. Res. Bull.* **47**, 3253 (2012).
- [48] J. Dai, J. Tang, H. Xu, L. Spinu, W. Wang, K. Wang, A. Kumbhar, M. Li, and U. Diebold, *Appl. Phys. Lett.* **77**, 2840 (2000).
- [49] A. C. Komarek, S. V. Streltsov, M. Isobe, T. Möller, M. Hoelzel, A. Senyshyn, D. Trots, M. T. Fernández-Díaz, T. Hansen,

- H. Gotou, T. Yagi, Y. Ueda, V. I. Anisimov, M. Grüninger, D. I. Khomskii, and M. Braden, *Phys. Rev. Lett.* **101**, 167204 (2008).
- [50] P. A. Bhowe, A. Chainani, M. Taguchi, R. Eguchi, M. Matsunami, T. Ohtsuki, K. Ishizaka, M. Okawa, M. Oura, Y. Senba, H. Ohashi, M. Isobe, Y. Ueda, and S. Shin, *Phys. Rev. B* **83**, 165132 (2011).
- [51] S. V. Streltsov, M. A. Korotin, V. I. Anisimov, and D. I. Khomskii, *Phys. Rev. B* **78**, 054425 (2008).
- [52] K. Schwarz and P. Blaha, *Comput. Mater. Sci.* **28**, 259 (2003).
- [53] P. Blaha, K. Schwarz, P. Sorantin, and S. Trickey, *Comput. Phys. Commun.* **59**, 399 (1990).
- [54] H. Taguchi, Y. Masunaga, K. Hirota, and O. Yamaguchi, *Mater. Res. Bull.* **40**, 773 (2005).
- [55] J. A. Alonso, J. L. García-Muñoz, M. T. Fernández-Díaz, M. A. G. Aranda, M. J. Martínez-Lope, and M. T. Casais, *Phys. Rev. Lett.* **82**, 3871 (1999).
- [56] M. Medarde, M. T. Fernández-Díaz, and P. Lacorre, *Phys. Rev. B* **78**, 212101 (2008).
- [57] T. Arima, Y. Tokura, and J. B. Torrance, *Phys. Rev. B* **48**, 17006 (1993).
- [58] S. K. Panda, I. Dasgupta, E. Şaşıoğlu, S. Blügel, and D. D. Sarma, *Sci. Rep.* **3**, 2995 (2013).
- [59] S. K. Panda, S. Bhowal, A. Delin, O. Eriksson, and I. Dasgupta, *Phys. Rev. B* **89**, 155102 (2014).
- [60] P. A. van Aken, B. Liebscher, and V. J. Styrsa, *Phys. Chem. Miner.* **25**, 323 (1998).
- [61] S. Biermann, L. de' Medici, and A. Georges, *Phys. Rev. Lett.* **95**, 206401 (2005).